TECHNICAL ARTICLE

Refurbishment of Continuous Caster Rolls by Laser Cladded Fe-Cr-Ni-Mo-Co Alloy

Nachiketa Yadav, Kumar Harsh, Harshad Natu, Kaushal Kishore, Arnab Karani, and Debalay Chakrabarti

Laser cladded low carbon 12Cr-5Ni-3Mo-5Co-based Fe powder system has been implemented to improve the performance of the vertical section rolls. Compositional, microstructural, and mechanical characterizations of the cladding and substrate materials were carried out as part of the development work. The electron probe microanalyzer was used to observe the distribution of important chemical elements in the clad region. The hardness value of clad region containing almost 100% martensitic structure was found ∼ 1.5 times more than the substrate value. The dilatometry test conducted within the temperature range from 100 to 700 °C shows that the coefficient of linear thermal expansion was lower for clad part than the substrate. Oxidation test was carried out at three different temperatures (200, 400, and 600 °C), where results showed that clad part possesses much better oxidation resistance than the substrate. Wear test carried out at 400 °C showed that wear loss for clad material is comparatively smaller than that of the roll material. It was found that the applied laser cladded system offers a good combination of hardness, oxidation resistance, and wear resistance compared to the conventional martensitic stainless steels (X20Cr13 grade).

1. Introduction

Continuous caster rolls (CCR), utilized for processing and transferring the slabs during solidification, are key components in steel manufacturing process and greatly influence steel production (Ref 1). In the continuous casting process, molten metal is poured from the ladle into the tundish, followed by a mold cavity through a submerged entry nozzle, where water cooling is used to solidify a shell of a sufficient thickness. The shell is withdrawn from the bottom of the mold through a series of caster rolls, and then it is subjected to water spraying to promote solidification (Ref 2-4). Mold flux is used to keep the molten metal from adhering to the copper mold plates. The mold flux containing CaF_2 reacts with water, creates an acidic environment, and enhances corrosion on the roll surface (Ref 5). Thus, the rolls are exposed to harsh service conditions, such as high slab contact pressure (ferro-static pressure) (Ref 6), abrasive wear from oxides and slag, cyclic thermal and

mechanical stresses, and high-temperature corrosion (Ref 7). These factors, individually or in combination, may lead to surface deterioration of the rolls.

Martensitic stainless steel (MSS) has been widely used as a roll material because of its fair thermal stability, corrosion resistance, and good wear properties at high temperatures (Ref 8). Although MSS possesses a combination of good wear and corrosion resistance, sensitization phenomena are favorable in the 400-600 °C temperature range. Therefore, with an increasing modernization of the continuous casting process, attention should not only be paid to improve properties of steel products, but also the equipment through which these steel products are produced. Surface modification techniques are one of the techno-economic approaches to increase the life of various equipment in different process industries including integrated steel plants. In this regard, deposition of WC in Fe matrix through hard-facing route enhanced the three-body wear resistance and service life of coal crushing hammer heads (Ref 9).

Several surface modification techniques are available, such as chemical vapor deposition, physical vapor deposition, thermal spray methods, submerged arc welding, plasma transferred arc cladding (Ref 10). However, laser cladding is preferentially used to produce an excellent metallurgical bond with less thermal distortion and porosity between the substrate and clad part. Compared with other conventional cladding methods, the advantages of using laser cladding are low dilution, small heat-affected zone (HAZ), great processing flexibility, and possibilities of selectively cladding small areas (Ref 11-13). Navas et al. (Ref 14) used laser surface treatments using two different clad materials AISI M2 and AISI 431 to improve wear resistance of mold steel. They reported that AISI M2 showed greater wear resistance than the clad AISI 431 because of its dense network of carbides. Kwok et al. (Ref 15) reported enhanced corrosion resistance due to the dissolution or

Nachiketa Yadav and **Debalay Chakrabarti**, Department of Metallurgical and Materials Engineering, Indian Institute of Technology, Kharagpur 721302, India; **Kumar Harsh**, Department of Metallurgical and Materials Engineering, National Institute of Technology, Karnataka 575025, India; **Harshad Natu**, Magod Fusion Technologies Pvt. Ltd., Maharashtra 411026, India; and **Kaushal Kishore** and **Arnab Karani**, Research and Development, Tata Steel Limited, Jamshedpur 831001, India. Contact e-mail: nachiketa20@kgpian.iitkgp.ac.in.

refinement of carbide particles and the presence of retained austenite after laser surface melting of AISI 440C martensitic stainless steel. Feng et al. (Ref 16) used and compared laser cladding and shielded metal arc welding for Inconel 625 coatings. They found improved high-temperature hardness and wear resistance of Inconel 625 coating by laser cladding because of the finer microstructure and alleviated segregation in the clad region.

Many attempts have been made to increase the life of continuous casting rollers. Viňáš et al. (Ref 1) used weld wires as a filler material to clad rolls using submerged arc surfacing and reported excellent wear resistance because of dispersion strengthening caused by finely dispersed carbides and nitrides in the weld coating. Ray et al. (Ref 17) suggested that laser cladding using Ni-based powder improves the service life of lateral rolls in a continuous casting machine. Maruschak et al. (Ref 18) modeled a temperature field at different points on the roll radius and observed that the thermal profile becomes smoother with an increase in distance from the surface. Lee

et al. (Ref 19) concluded that a geometrically constrained structure like a cylindrical roll under cyclic stresses is more prone to thermal fatigue, as thermal expansion and contraction occur in the CCR during cyclic heating and cooling conditions.

Although, there are several attempts to improve service life and performance of continuous caster rolls, most of the reported works involve the use of expensive overlay alloys such as nickel based super alloys on new caster rolls. In the present work, a novel and cost-effective low carbon 12Cr-5Ni-3Mo-5Co iron-based alloy is deposited through laser cladding route

Table 1   Chemical composition of substrate and powder material in weight percentage

Element	Base material	Overlay
C	0.15	0.015
Cr	12.5	12.1
Ni	0.5	5.1
Mn	0.69	0.31
Mo	0.3	2.86
Co	–	4.57
Si	0.4	0.64
S	0.008	0.001
P	0.02	0.016
Fe	Balance	Balance

Table 2   Optimized process parameters for laser cladding

Power (W)	1700
Stand off distance (mm)	23
Powder (g/s)	0.5833
Nozzle gas (l/s)	0.25
Step over (mm)	1
Speed (mm/s)	25
Carrier gas (l/s)	0.25

Table 3   Chemical composition of slurry

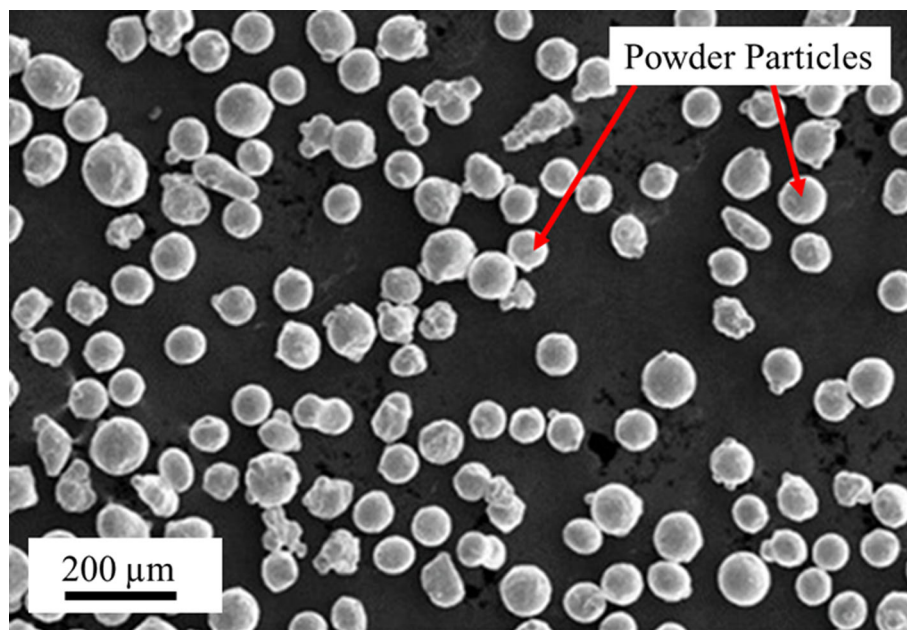| Constitutents	Percentage distribution
CaO	34
SiO_2	40
Al_2O_3	5
$Na_2O + K_2O$	10
F	11

Fig 1   Micrograph of gas atomized low carbon 12Cr-5Ni-3Mo-5Co-based Fe powder particles

for refurbishment of discarded rolls. It is worth noting that in many cases, caster rolls made of X20Cr13 grade martensitic stainless steel without any overlay cladding is used in this application. During service, these rolls suffer from surface damage due to oxidation and high-temperature wear. The present work aims at evaluating the suitability of a laser cladded low carbon 12Cr-5Ni-3Mo-5Co Fe-based alloy for the purpose of refurbishment. Therefore, a detailed comparison of laser cladding of this alloy with the existing caster roll is conducted with respect to the properties required for the application, viz., coefficient of thermal expansion, hardness, high-temperature wear resistance, and oxidation resistance. Further, the mechanism of improved wear resistance and oxidation of the cladding is attributed to the composition and the microstructure of the cladding.

2. Experimental Procedure

2.1 Roll and Clad Materials

The as-received rolls (base material), quenched and tempered at 800 °C, were manufactured from X20Cr13 grade martensitic stainless steel. Low carbon 12Cr-5Ni-3Mo-5Co Fe-based alloy powder resembling super martensitic stainless steel (SMSS) composition was selected to clad the roll surface by laser cladding techniques. The chemical composition of substrate and powder, as presented in Table 1, was determined by optical emission spectroscopy (OES). Powder particles, almost spherical in shape (ranging from 75 to 100 μm), as shown in Fig. 1, were prepared using the gas atomization technique.

Table 4 Test conditions for wear analysis

Load, N	50
Frequency, Hz	5
Duration, min	34
Temperature, °C	400
Stroke, mm	5

2.2 Materials Characterization

The coupon samples were prepared from the continuous caster roll (CCR) with dimensions 200 × 80 × 20 mm using DCM-340, a double-column heavy-duty band saw machine. Prepared samples were thoroughly cleaned with ethanol, followed by a dye penetration test (DPT) to inspect any crack present on the surface. Samples that passed the DPT were taken for laser cladding. The laser cladding was performed using a continuous diode laser and a powder feeding system, where the laser beam was guided through a fiber system and focused on the surface of the substrate material perpendicularly. Argon gas was used as a carrier gas for powder feeding and shielding gas for preventing oxidation. Laser had a maximum power output of 4 kW and laser beam spot size on the surface of work-piece was fixed to 3 mm. All the parameters were optimized for the system before cladding to ensure the formation of laser cladding with minimal porosity ($< 0.5\%$). In order to develop a clad layer of thickness nearly 2 mm, deposition was carried out two times following a raster pattern. The optimized process parameters for laser cladding are listed in Table 2.

Surface grinding using a magnetic wheel grinder was used to polish the surface prior to tests. Small pieces having 20 × 20 mm cross section and 5 mm thickness were cut out from these plates and mounted using bakelite for microstructural analysis. For etching, Kalling's Number-2 reagent (5 g $CuCl_2$, 100 ml HCl and 100 ml ethanol) was used. The etched samples were examined under Leica(R) optical microscope and a Quanta(R) FEG 650 scanning electron microscope (SEM). Electron Probe Micro Analysis (EPMA) with 0.1 μm tungsten probe was performed on the cladded samples to get the elemental distribution of constituent phases. To identify the presence of different phases, samples were subjected to x-ray diffraction (XRD) analysis in a high-resolution x-ray diffractometer (X'Pert PRO, PANalytical B.V, PW3040/60, The Netherlands). Cu Kα radiation (λ = 1.54056 Å) was used for the XRD of both the substrate and the cladding alloy for the identification of phases. Vickers microhardness tests were performed using Leica microhardness tester at a load of 0.098 N and a dwell time of 13 s. Three line profiles across the cross section were measured for statistical accuracy to determine the variations of the hardness from the cladding to the substrate
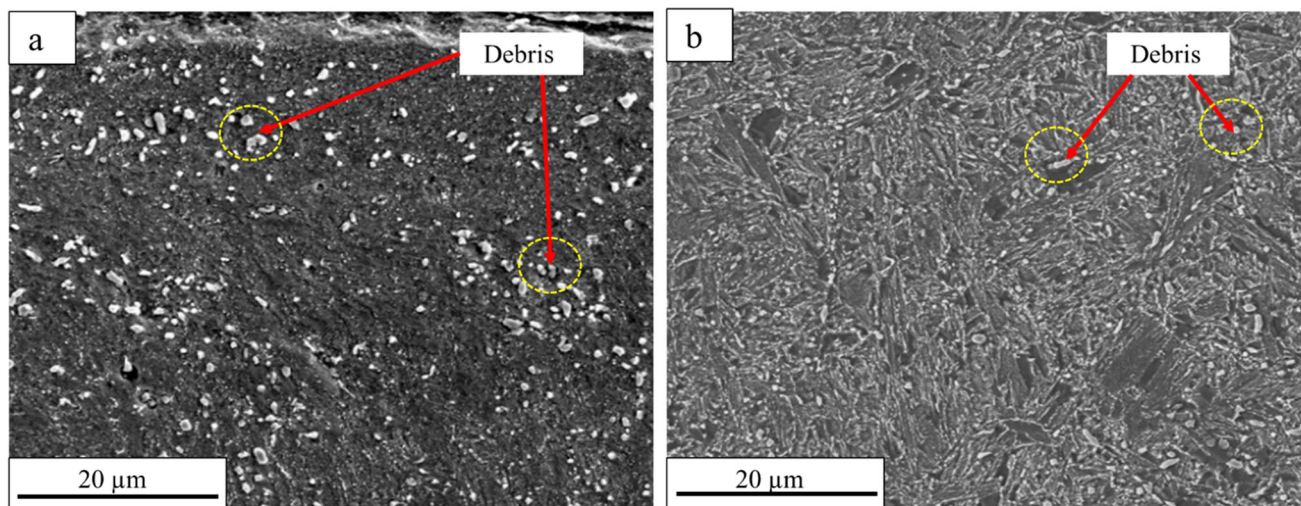

Fig 2 Microstructures taken under SEM for (a) outer cross section of discarded roll and (b) inner cross section of discarded roll
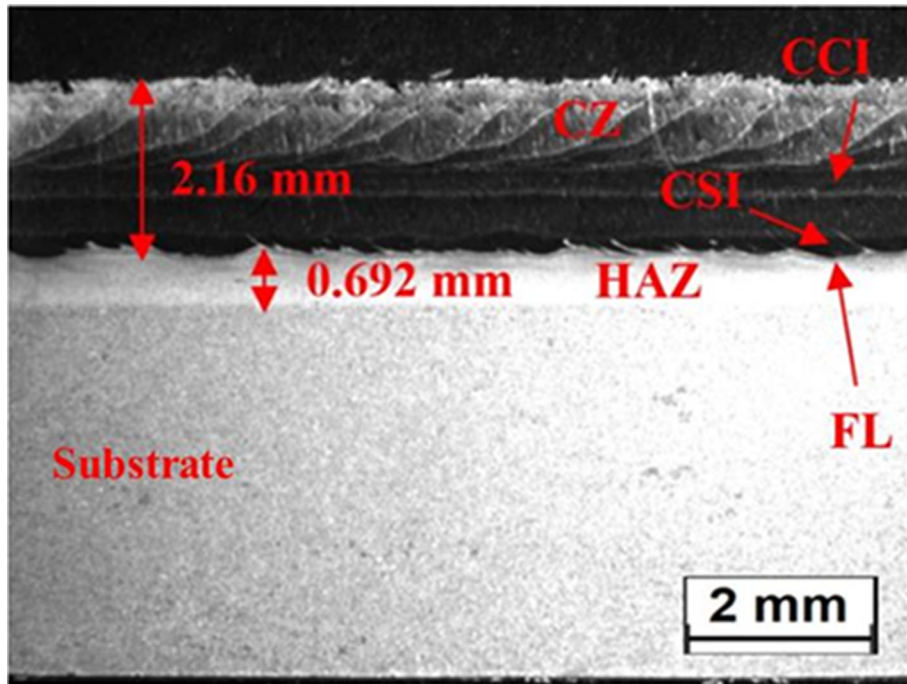
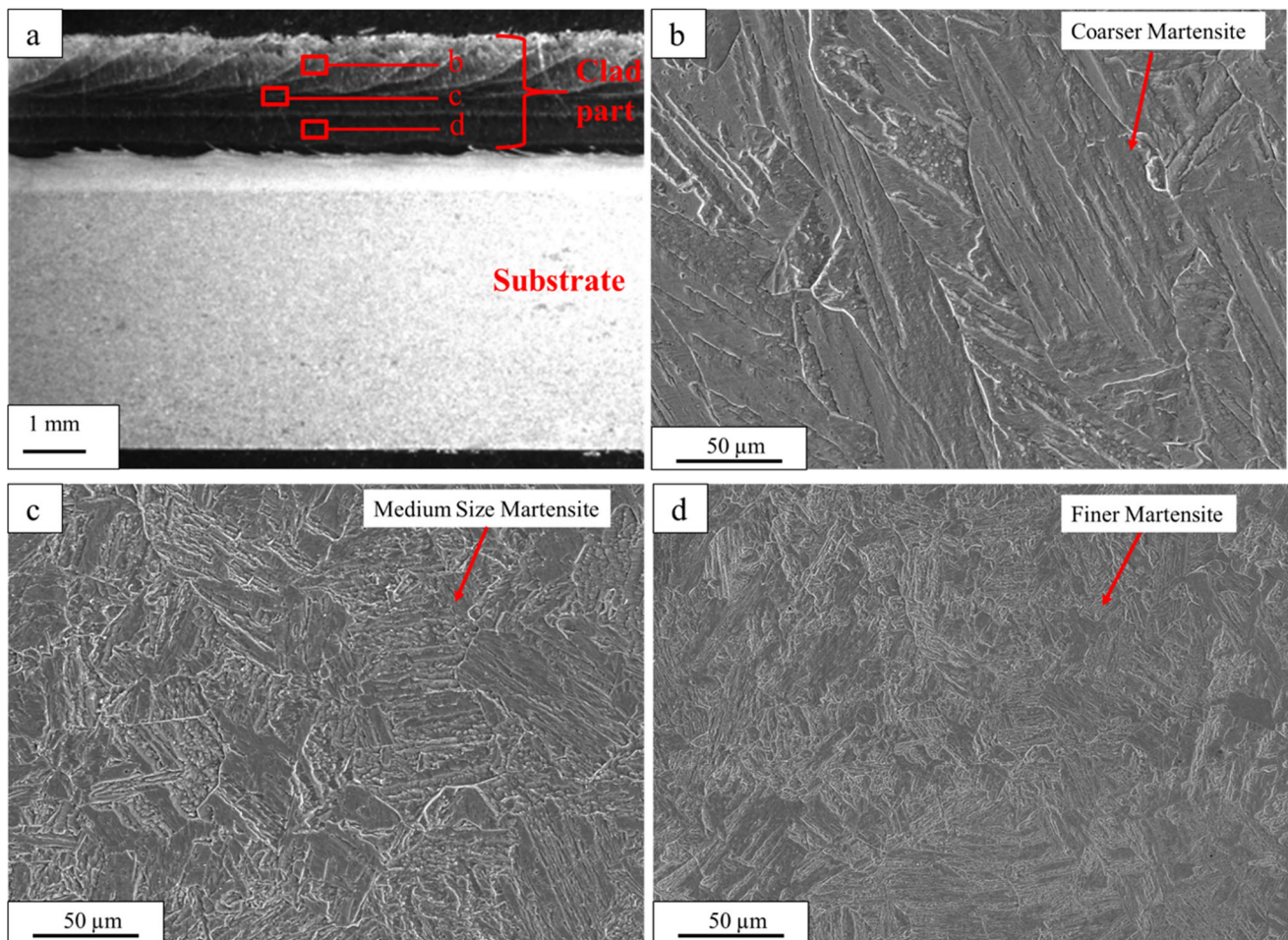**Fig 3** Stereo-macrograph showing different regions in clad and substrate

Fig 4 Microstructure of Fe-based clad (b) to (d), corresponding to different regions marked in macro-image a
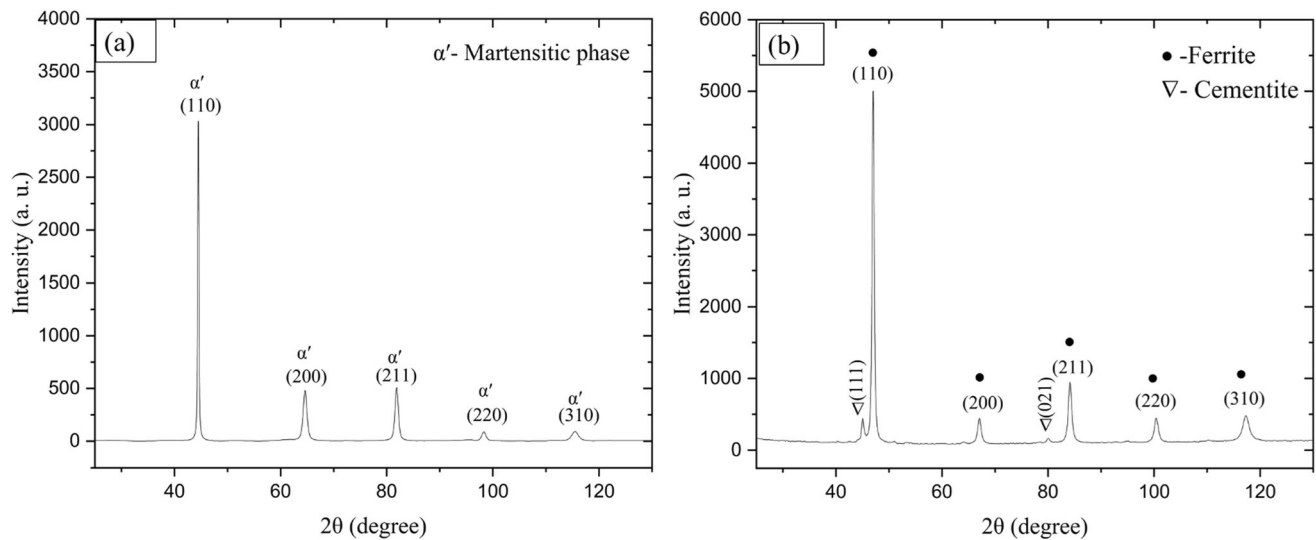
Fig 5 The XRD pattern of (a) clad and (b) substrate.

including dilution zone and heat-affected zone. The variation of coefficient of thermal expansion (CTE) with temperature for both substrates and clads are an important indicator of the thermal stresses that may develop during the operation. In general, the lower the CTE values at any given temperature, the smaller the thermal stress will be. CTE was studied under a contact type dilatometer equipped with thermomechanical simulator Gleeble® 3800. The sample was heated up to 700 °C at a rate of 10 °C/min, followed by cooling to room temperature at the same rate. The corresponding change in sample length was recorded. This change in length was then used to calculate the CTE value using equation (1), and the corresponding graphs were plotted.

$$\alpha = (1/L_0) \times (\Delta L/\Delta T) \qquad \text{(Eq 1)}$$

Where α = coefficient of thermal expansion, L_0 = initial length, ΔL = change in length, and ΔT = change in temperature.

Two different set of samples with dimensions that provide a surface area of 15×15 mm^2 and 20×20 mm^2 with a thickness of 5 mm were cut by electrical discharge machine (EDM) for both the cladded part and the substrate for oxidation and wear test, respectively. In order to standardize the sample surface, polishing of samples was done using silicon carbide sandpaper down to grit size 600. After that, the samples were cleaned with alcohol and dried with hot air. A muffle furnace was used to heat the samples for the high-temperature oxidation test. A model was developed to simulate the actual situation of rolls situated near the mold so that samples could come in contact with the acidic environment. For that purpose, a slurry (mixture of water and flux powder in the ratio of 70:30) was prepared and placed inside the crucible.

The samples were mounted on slurry and placed inside the muffle furnace with the crucible. The chemical composition and distribution of the slurry are presented in Table 3. The oxidation test was performed at three different temperatures (200, 400, and 600 °C) for clad and substrate materials. Heating and cooling rates were maintained at 5 °C/min, while homogenization time was fixed for 5 h at each test temperature. Elemental concentration profile by 'line-scan' method for the oxidized layer for both substrate and clad was performed using energy

dispersive spectroscopy (EDS) device equipped SEM. A linear reciprocating type tribometer was used for wear testing, operating at 400 °C for substrate and clad materials. The test was repeated for five samples (each for substrate and clad), keeping the same test conditions. Ball material used in the tribometer for testing was AISI 52100 Cr steel having a hardness value of 848 HV. Test conditions for wear analysis are given in Table 4.

3. Results and Discussions

3.1 Microstructural Analysis

Before cladding with low carbon 12Cr-5Ni-3Mo-5Co Fe-based powder, SEM images of outer and inner cross sections were taken of the discarded rolls, as shown in Fig. 2. It can be observed that the outer section of discarded rolls, which were in direct contact with partially solidified liquid steel, has been deteriorated more compared to the inner one.

Macrograph of cladding layer across the cross section, as presented in Fig. 3, shows that it consists of different regions, such as clad zone (CZ), clad-substrate interface (CSI), clad-clad interface (CCI), fusion line (FL), and heat-affected zone (HAZ). A very narrow HAZ (0.692 mm) was observed, as shown in Fig. 3, which is a characteristic feature of laser cladding and welding processes.

The micrographs obtained from different locations of clad are shown in Fig. 4. The microstructure of the clad part is martensitic. The XRD data of the clad are shown in Fig. 5(a), which also confirm fully martensitic phase. XRD data for the substrate are shown in Fig. 5(b). It consists of predominantly ferrite and cementite due to tempering of substrate. The difference in microstructure at different positions from top to bottom (toward substrate) can be explained from relation between the temperature gradient and solidification rate. In the clad region near the substrate, the solidification rate is high because the substrate acts as a heat sink, and hence, the temperature gradient is high (Ref 20). Therefore, the microstructure at location d, denoted in Fig. 4, is finer. Moving upward direction in the clad region away from the substrate
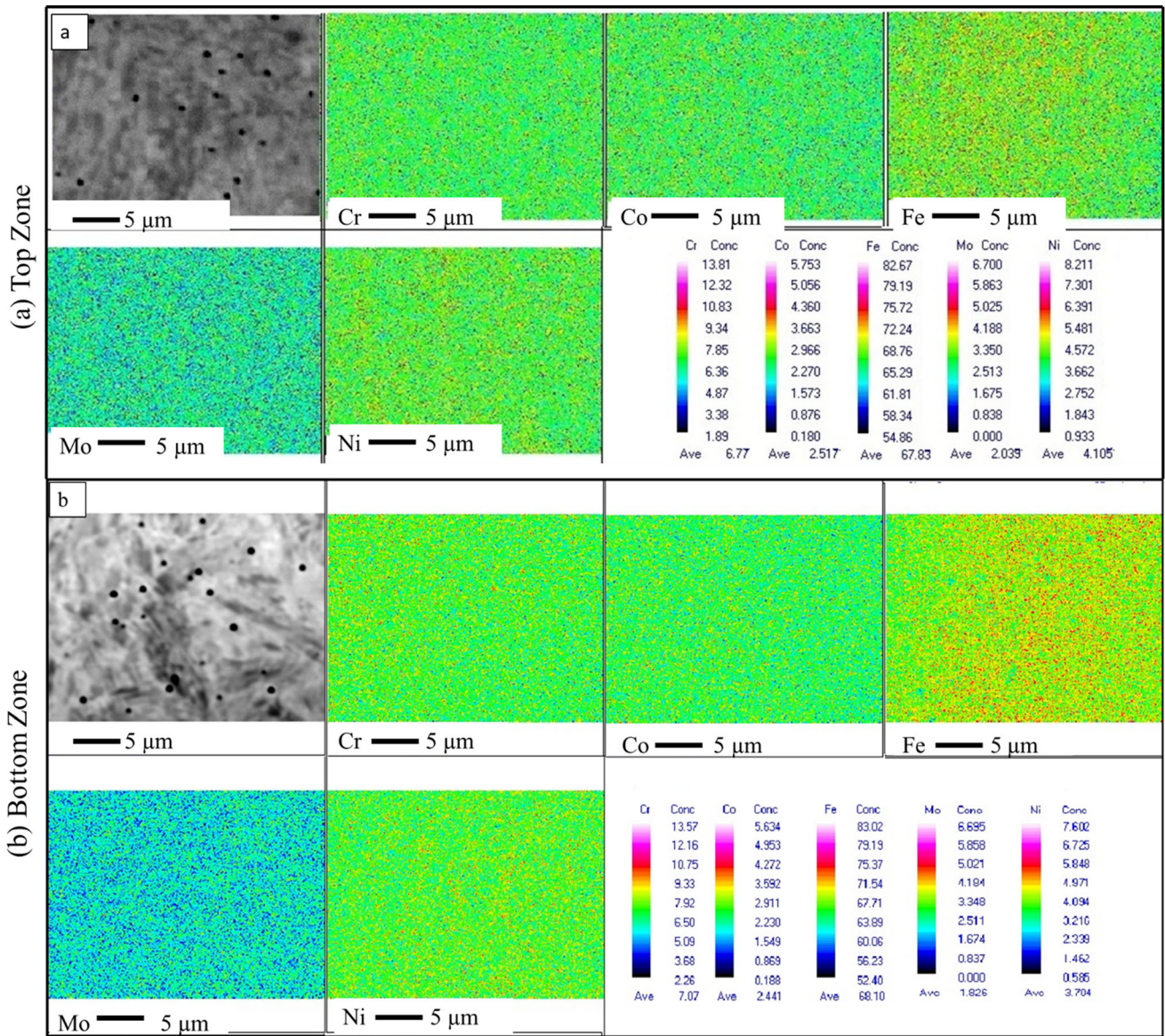
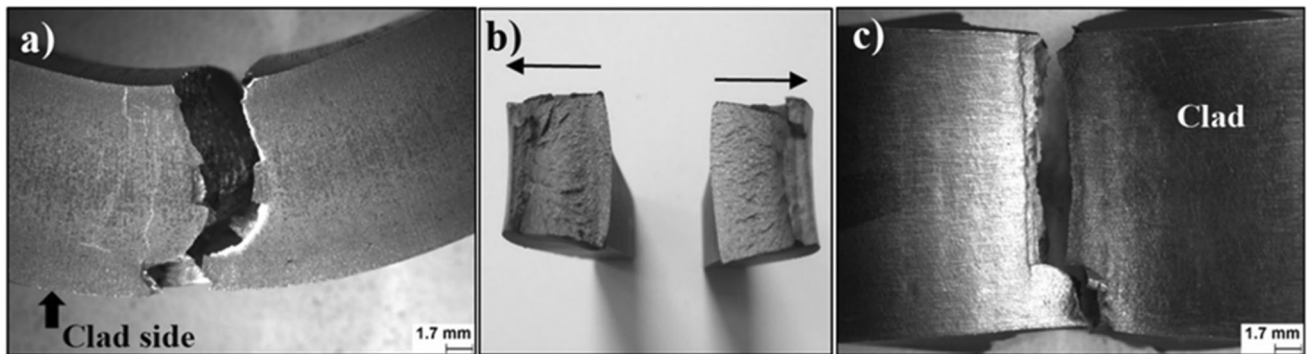**Fig 6** EPMA analysis for (a) top zone and (b) bottom zone of clad region

Fig 7 Images of cladded sample after bend test (a)-(c), where (a) side view, (b) fracture surfaces, and (c) top view of clad
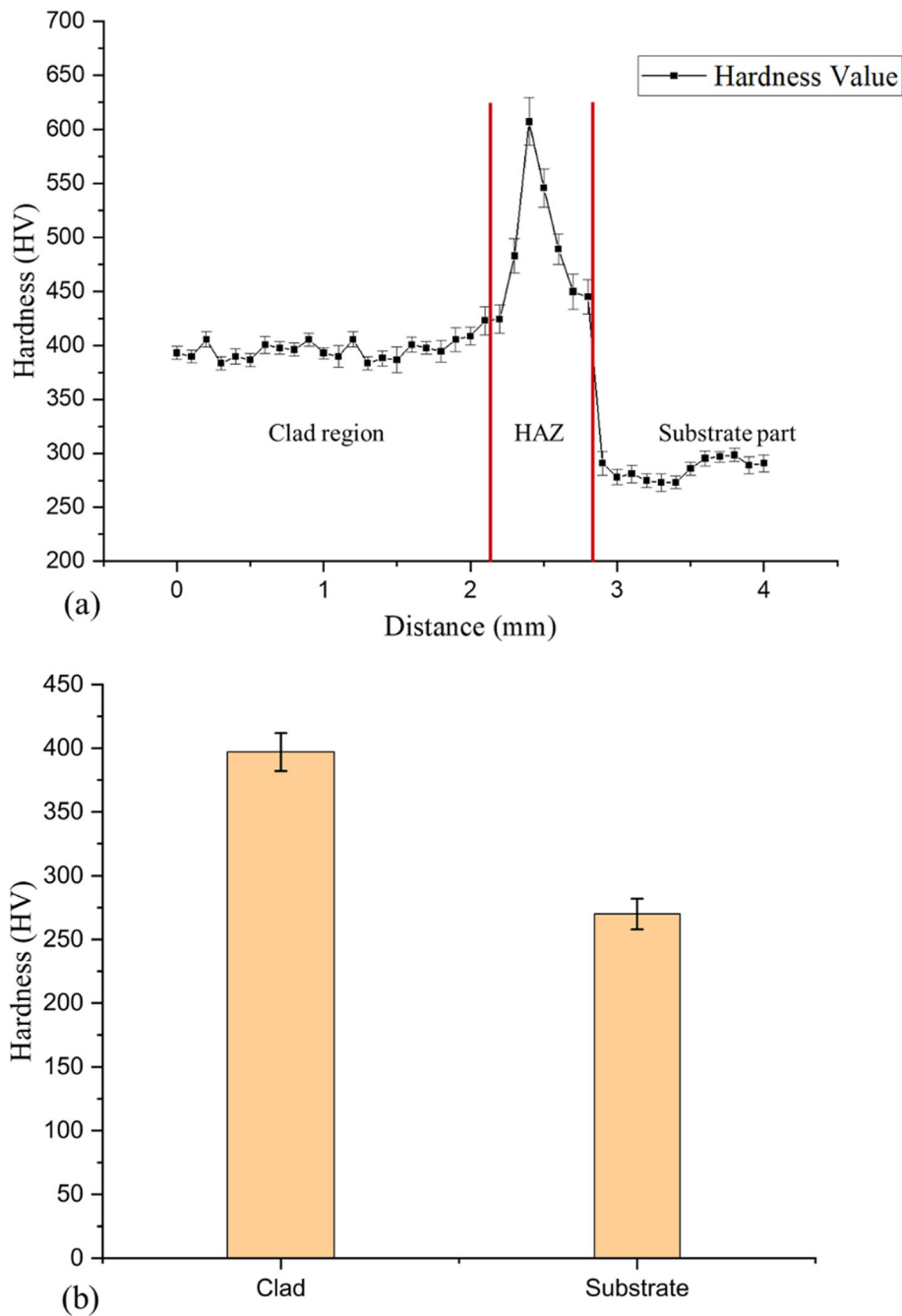
Fig 8 (a) Microhardness profile of specimen as a function of distance for the laser cladded specimen and (b) hardness comparison for clad and substrate

(from location d to b in Fig. 4(a)), both temperature gradient and solidification rate get reduced compared to near the substrate region, and as a result, a coarser microstructure is observed.

The results of electron probe microanalysis (EPMA) conducted in the top and bottom zone of the clad are shown in Fig. 6. The elemental distribution is almost uniform. However, a slight decrease in the concentration of alloying elements like Mo, Ni, and Co can be observed in the bottom zone, while Fe concentration increases slightly. It indicates the presence of dilution in the clad. Further, there is no sign of carbide formation in the matrix, which is consistent with the microstructural study using SEM and XRD.

3.2 Bend Test and Microhardness Measurements

A 3-point bend test was used for the sole purpose of qualitative analysis of clad samples, which includes examining the compatibility of the clad track with the substrate. If there is any discrepancy in the metallurgical bond achieved by laser cladding, it is expected to observe delamination of the clad layer at the clad-substrate interface. Figure 7 shows images of bend samples at different angles after completing the test. It can be concluded that the metallurgical bond between the clad and
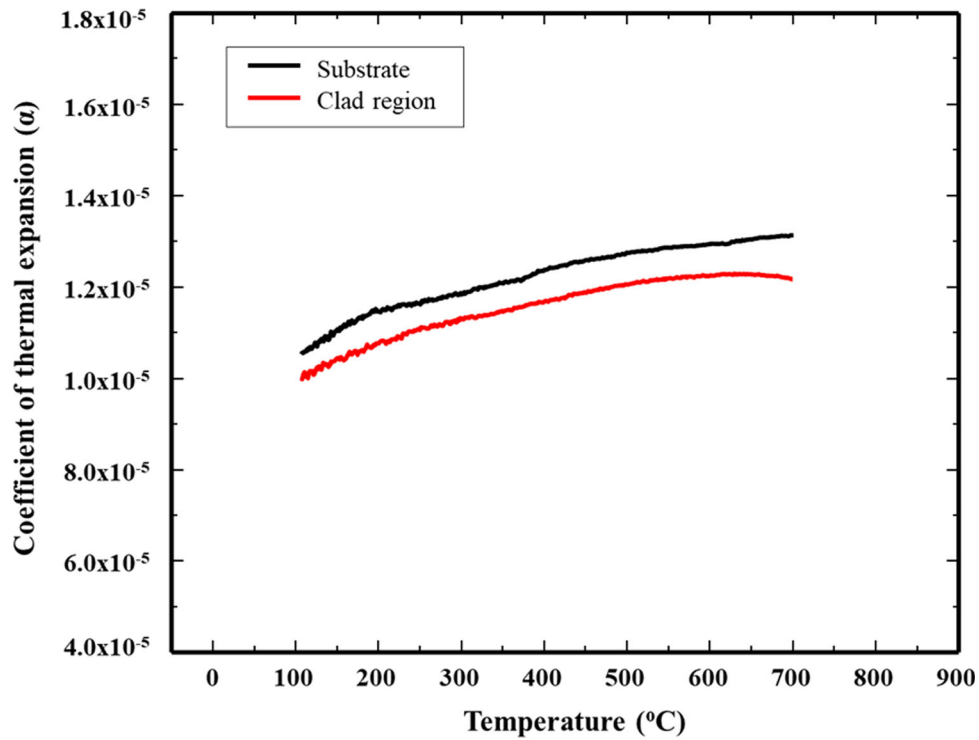
Fig 9 The variations of coefficient of thermal expansion (CTE) with temperature for both substrate and clad samples
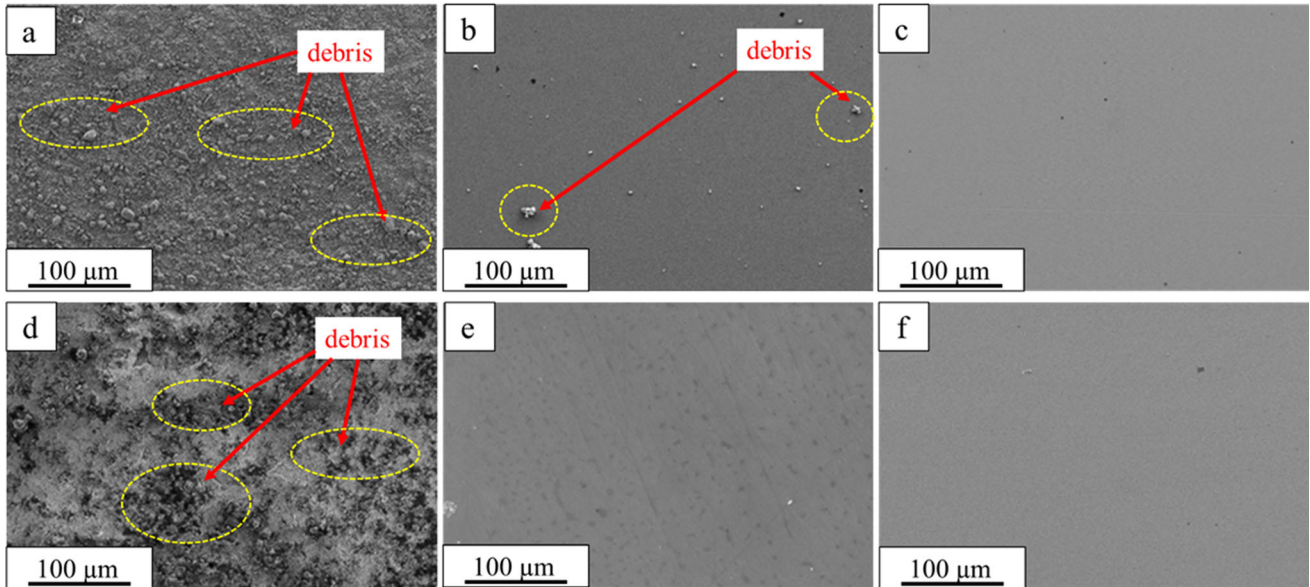

Fig 10 SEM images of surface layer for the substrate (a) to (c) and the clad samples (d) to (f) after oxidation tests at three different temperatures, 600 °C (a) and (d), 400 °C (b) and (e), and 200 °C (c) and (f)

the substrate is good as no delamination at the interface is observed.

The microhardness profile showing three different regions: clad region, heat-affected zone and substrate for the laser cladded specimen is plotted in Fig. 8(a). The hardness value of the clad varies over the range of 380-430 HV, which is comparatively higher than the roll material, X20Cr13 (260-280 HV). The comparison in hardness of clad region and roll material is shown in Fig. 8(b). The formation of the refined martensite because of very fast cooling due to laser

cladding technique can generate Hall-Petch strengthening, which significantly enhances the micro-hardness. A similar study regarding an enhanced hardness in the laser cladding and other laser-based direct energy deposition route was reported for various alloys (21-23). Melting the top region of the substrate (near the clad-substrate interface) is necessary for superior bonding between clad and substrate. Therefore, the temperature of HAZ in laser cladded specimen increases, and it goes above the upper critical temperature into the fully austenitic region due to heat absorbed by the base material.
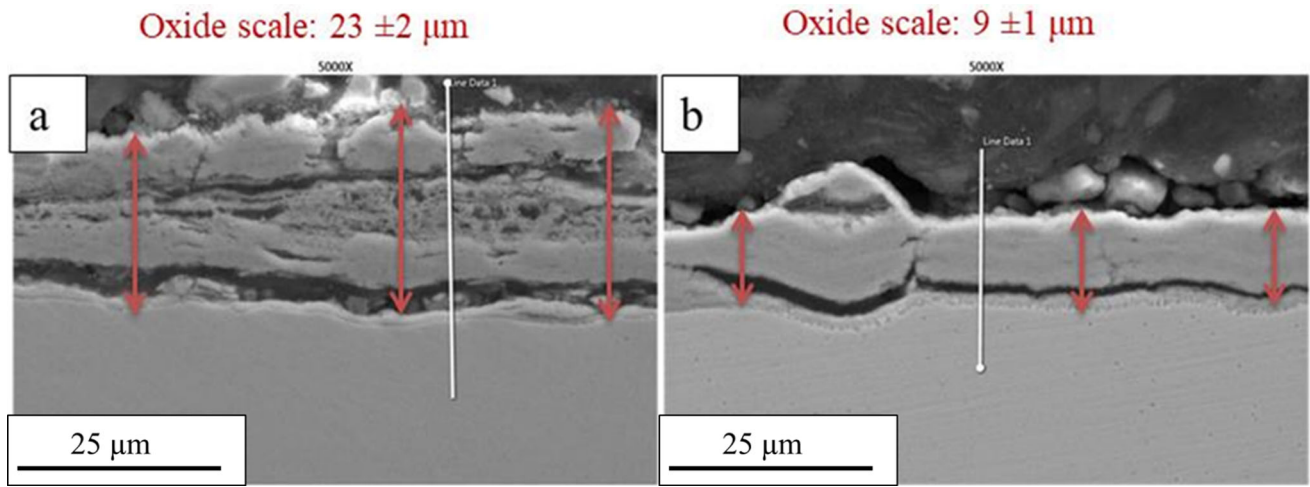
Oxide scale: 23 ±2 µm   **Oxide scale: 9 ±1 µm**

Fig 11 Cross-section showing oxide scale layers for both (a) substrate and (b) clad samples after oxidation at 600 °C
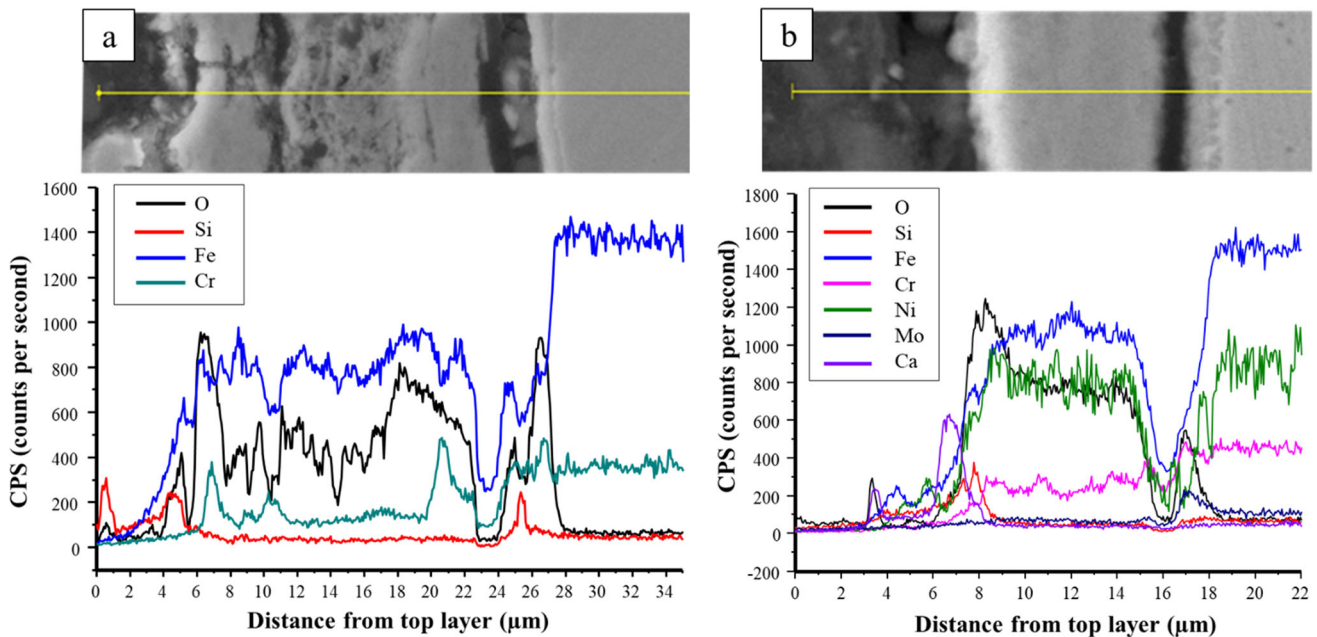

Fig 12 Elemental concentration profile by 'line-scan' method through EDS analysis for both (a) substrate and (b) clad samples after oxidation at 600 °C

Since most of the carbon would have gone back into solution in the austenite phase, it transformed to fully fresh martensitic structure with a high amount of carbon content upon cooling, which may be the reason for the HAZ hardness reaching 620 HV. For the laser cladded specimen, the hardness of substrate varies between 260 and 280 HV. The lower hardness value is because of tempering of substrate part before overlaying the clad. Tempered martensitic microstructure is essential for the substrate to ensure adequate toughness.

3.3 Dilatometry Test

The coefficient of linear thermal expansion (CTE) is a measure of fractional increase in the length of a component per unit temperature change. For a constrained geometry like a cylinder operating in cyclic temperature variation, CTE is one prime concern that needs to be evaluated to avoid failure. The lower the value of CTE, the lower the thermal stresses generated in the component will be, which can result in a higher structural stability and reduce the tendency of thermal fatigue failure. However, the difference in the CTE values between the cladding and substrate should not be too large to avoid any possibility of failure from the cladding/substrate interface. For development of low thermal expansion in ferritic/martensitic or austenitic stainless steels, alloying elements such as Co, Ni are added to the material as they increase the interatomic distance and thus decrease the bond energy between iron-iron atoms (Ref 24). Hull et al. (Ref 25) compiled the data on the effect of different alloying elements in thermal expansion for ferritic/martensitic stainless steels and suggested that addition of Co and Ni in ferritic/martensitic stainless steel decreases the coefficient of thermal expansion values. As
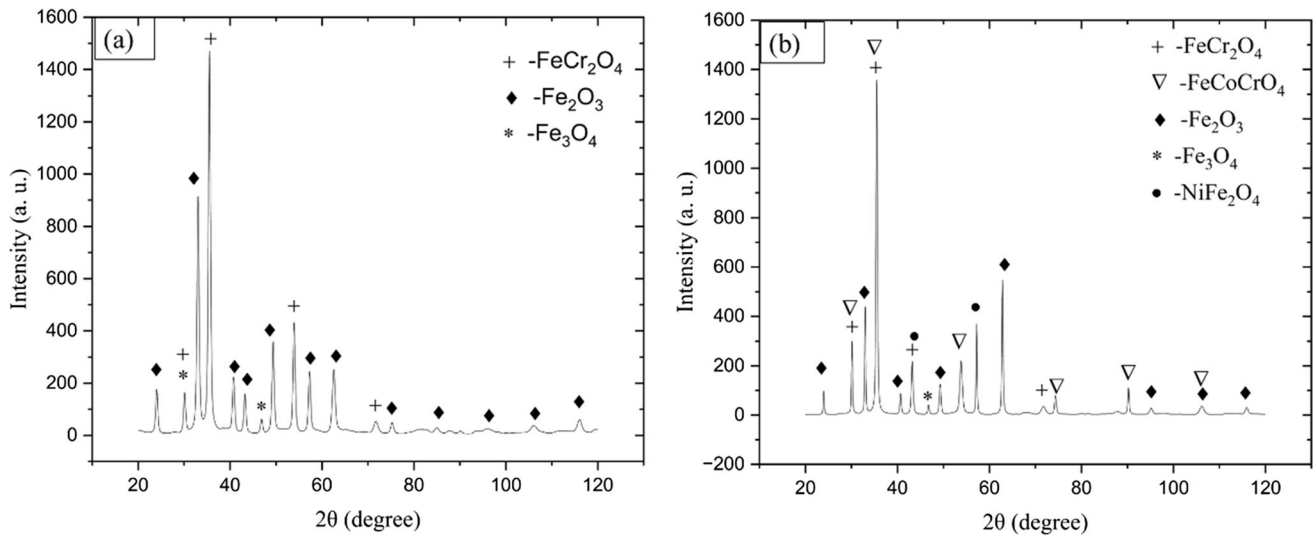
Fig 13 Phase analysis of XRD pattern for both (a) substrate and (b) clad samples after oxidation at 600 °C
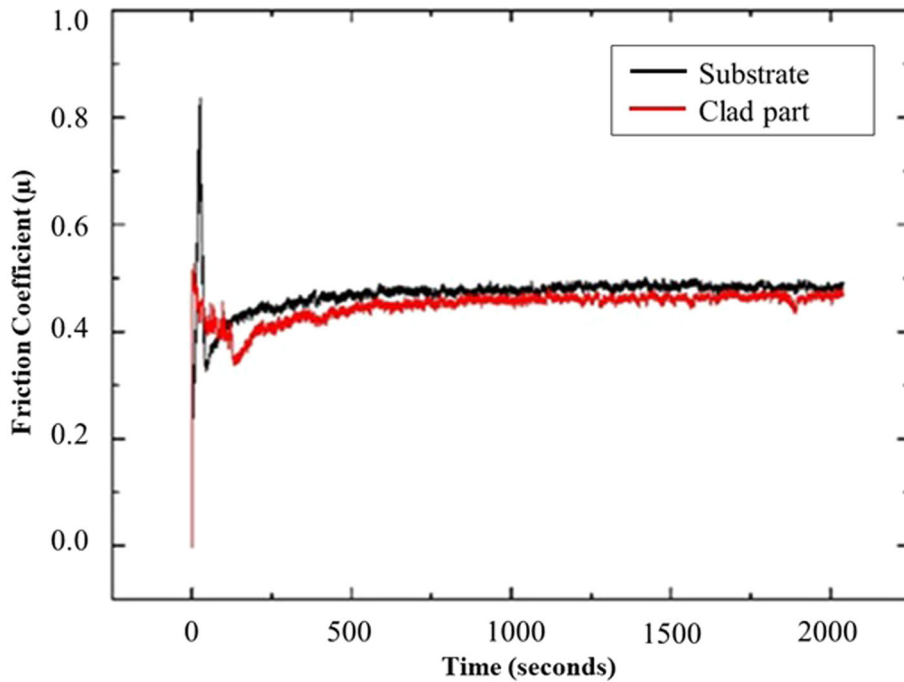

Fig 14 The variations of friction coefficient for substrate and clad samples during wear test at 400 °C

shown in Fig. 9, the CTE versus temperature graph was obtained in a contact type dilatometer. The clad region shows slightly lower CTE values at all tested temperatures compared to the substrate and hence, it is expected to experience lower thermal stresses in the cladding region during thermal fluctuation in the service condition. Clad was alloyed with Co and Ni, which is a differentiating cause for a decreased level of CTE compared to the substrate. However, the CTE values of cladding were only marginally lower than the substrate. Therefore, the level of thermal stresses is expected to be low in cladding/substrate interface due to a comparable thermal CTE values of cladding and substrate.
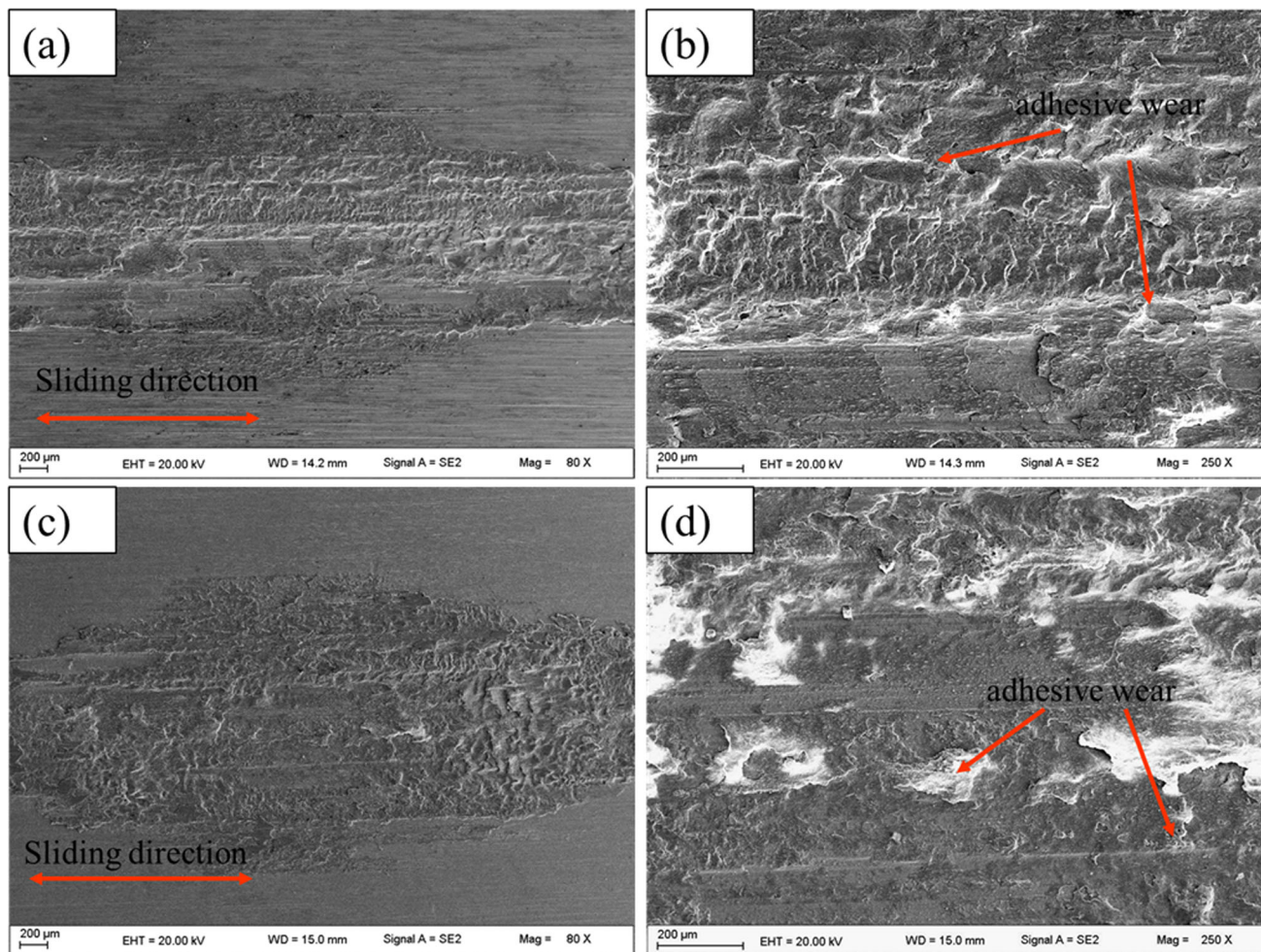
Fig 15 SEM micrograph of wear tracks for (a), (b) substrate and (c), (d) clad samples

3.4 Oxidation Behavior

The surface layer SEM images for the substrate and clad region after oxidation tests are shown in Fig. 10. Oxidation of samples increases with increasing temperature (Ref 3); hence, more debris can be seen at higher temperature (600 °C) compared with that at 200 °C and 400 °C because of unstable oxide film at higher temperature. The oxidation scale for the clad, which is considerably thinner (9 ± 1 μm at 600 °C) compared to the substrate (23 ± 2 μm), is shown in Fig. 11. Elemental distribution by line-scan through EDS analysis was also conducted. The concentration profiles for oxygen, iron, chromium and the other alloying elements are shown in Fig. 12 for both the substrate and clad part. The phase identification using XRD pattern of both clad and substrate after oxidation at 600 °C is shown in Fig. 13. In clad sample, $FeCoCrO_4$ and $NiFe_2O_4$ phases were also observed along with $FeCr_2O_4$, Fe_2O_3 and Fe_3O_4. The presence of high-temperature alloying elements such as Cr, Co, Ni help in formation of stable and adherent oxides. These adherent oxides at high temperature reduce the diffusion of iron toward the outward direction and oxygen toward the inward direction and hinder the formation of non-porous iron oxides (Ref 26, 27). Therefore, oxidation of clad occurs to a smaller extent compared to the substrate material.

3.5 Wear Test

The wear test was carried out at 400 °C to evaluate the wear resistance of the clad and the substrate materials. Higher wear rate for substrate (0.00075 ± 0.00005 mm^3/m) than clad (0.00040 ± 0.00002 mm^3/m) was observed. The variations of friction coefficient with time for both substrate and clad are plotted in Fig. 14. Initial instability and decrement in friction coefficient with time were observed in all samples. In the wear process, there are two stages: (1) wear-in stage (unstable wear) and (2) stable wear stage. The first one corresponds to the beginning of the test, where the friction coefficient is maximum and highly unstable. It may be due to the cold welding effect at the contact points of friction pairs, and as a result, the high shear force is required to abrade the interfacial film and cut the welded point (Ref 16, 28). Thereafter, the stable wear stage occurs with the first decrease in friction coefficient which then becomes almost stable. The decrement in friction coefficient can be attributed to the extent at which different wear mechanisms are involved at different time. The friction pair components (disk and sample) undergo adhesive and abrasive wear.

Wear-in-stage corresponds to mainly abrasive wear mechanism where friction coefficient is maximum and highly
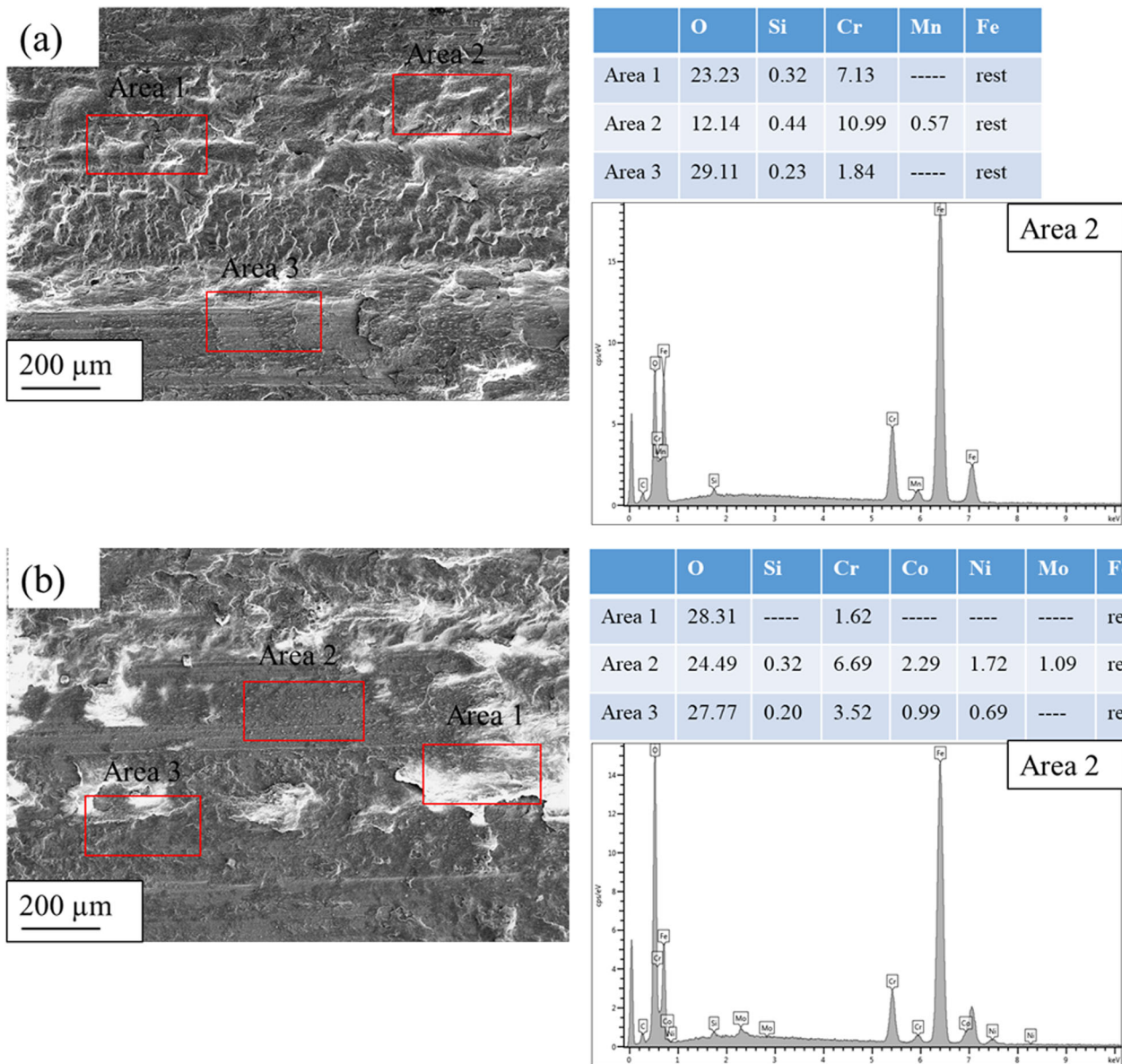
Fig 16 Selected area EDS analysis for elemental distribution (in wt.%) of (a) substrate and (b) clad samples after wear tests at 400 °C

unstable. While, stable wear stage corresponds to dominant adhesive wear mechanism. After abrasive wear mechanism where material is abraded and cut, adhesive wear is dominant where transfer of abraded material between friction pairs takes place. For both clad and substrate materials, it can be noted that wear-in stage (stage 1) is slightly longer (in Fig. 14) because the cold welding effect may be aggravated initially at high temperatures (Ref 16). SEM images of wear-tested substrate and cladded specimens are shown in Fig. 15. Both the substrate and cladded specimens revealed the formation of oxide layers after wear testing confirming adhesive wear between oxide layer on the specimens and the counter-body surface to be the dominant mechanism of wear. It is evident that the extent of deformation and damage of worn-out surface in case of substrate is greater compared to the cladding. This is consistent with the formation of more adherent oxide layers in cladded specimen as also evident from the oxidation results. Further, EDS analysis of the worn-out surface revealed the presence of Co, Cr and Ni in the oxide of cladded specimen as shown in Fig. 16. An adherent oxide layer can act as a lubricant and would reduce both the coefficient of friction and the wear volume loss (Ref 29, 30). Additionally, a higher hardness of the cladding compared to the substrate may also contributed to its improved wear resistance.

The wear surface profile at 400 °C was further investigated using a confocal laser scanning microscope, as shown in Fig. 17. The debris deposition, shown as the red region, is more extensive at the substrate than the clad part. This can be attributed to an increased rate of adhesive wear for the substrate than the clad material at high temperatures.
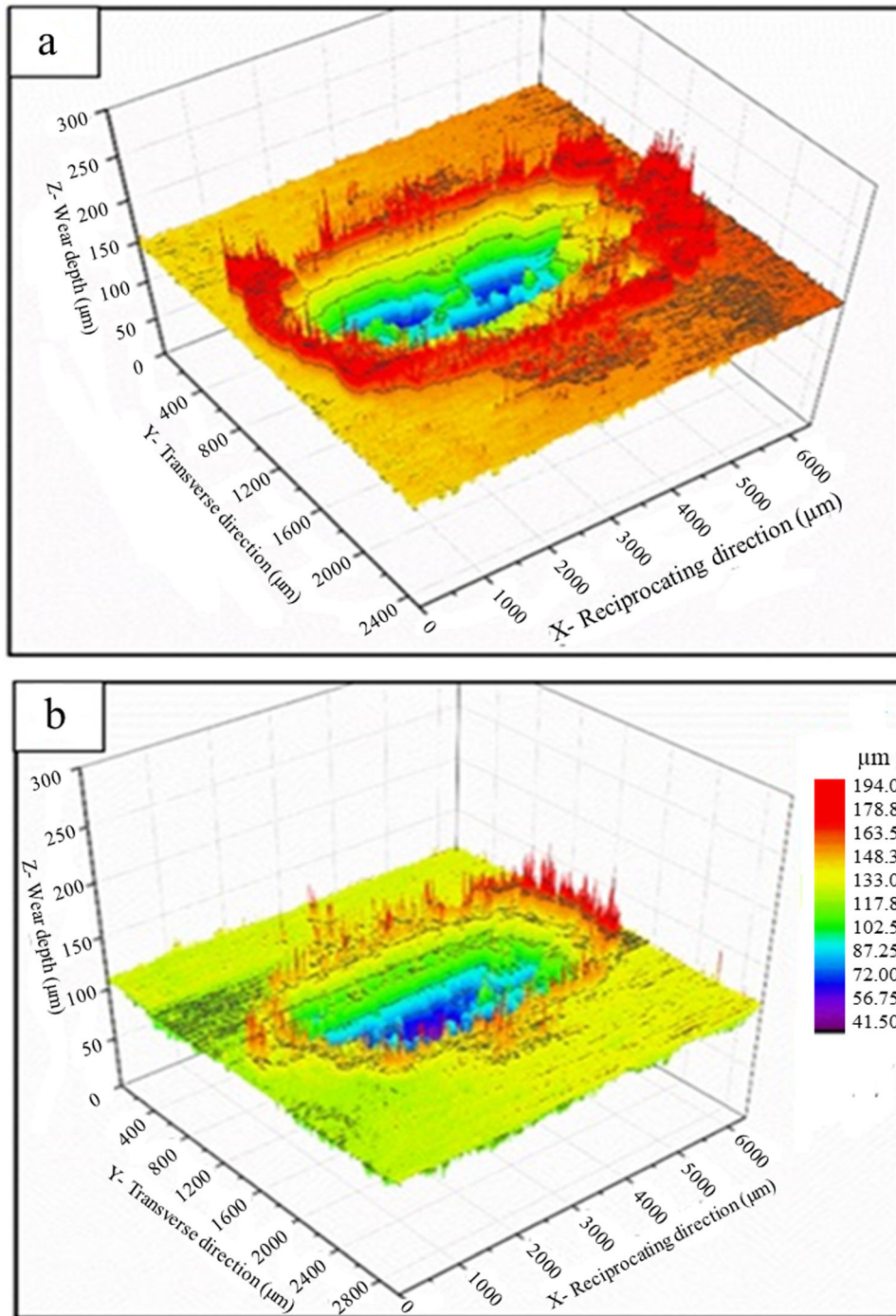
Fig 17 Wear surface profiles of (a) substrate and (b) clad samples after wear tests at 400 °C

4. Conclusions

With an attempt to improve life of rolls in vertical section in continuous casting machine, martensitic stainless steel grade (X20Cr13) roll was cladded using low carbon 12Cr-5Ni-3Mo-5Co Fe-based powder by laser cladding. The important findings from this work are as follows:

1. The low carbon 12Cr-5Ni-3Mo-5Co-based Fe powder resembling super martensitic stainless steel (SMSS) composition offers a superior combination of hardness, oxidation resistance and wear resistance compared to the conventional martensitic stainless steels (X20Cr13 grade).
2. The EPMA test shows almost uniform elemental distribution in the clad regions, while 3-point bend test shows no delamination at the interface of clad and substrate after laser cladding.

3. The hardness value of the clad region containing $\sim 100\%$ martensitic structure was ~ 1.5 times more than that of the substrate. This is possibly due to the rapid solidification arising from the laser cladding process resulting in finer martensitic microstructure.

4. The clad shows a lower coefficient of linear thermal expansion (CTE) at all tested temperatures compared to the substrate. The reduced CTE is beneficial from the viewpoint of reduction in thermal stresses due to temperature fluctuation during the operation of the caster rolls.

5. The oxidation scale thickness was 9 ± 1 μm for the clad material and 23 ± 2 μm for the substrate, indicating better oxidation resistance in the former case. The high temperature resistant alloying elements (such as Ni and Co) in clad region help in the formation of stable oxides at high temperatures as confirmed by XRD analysis.

6. The formation of stable oxides coupled with a higher hardness of the cladding resulted in an improved adhesive wear resistance compared to the substrate.

Author Contribution

NY: Conceptualization, Data curation, Investigation, Methodology, Writing–original draft. **KH**: Data curation, Investigation, Methodology. **HN:** Investigation, Methodology. **KK:** Data curation, Writing–review & editing. **AK:** Supervision, Writing–review & editing. **DC:** Supervision, Writing–review & editing.

Conflict of interest

The authors declare that they have no known competing financial interests or personal relationships that could have appeared to influence the work reported in this paper.

References

1. J. Viňáš, J. Brezinová, and A. Guzanová, Analysis of the Quality Renovated Continuous Steel Casting Roller, *Sadhana Acad. Proc. Eng. Sci.*, 2013, **38**(3), p 477–490. https://doi.org/10.1007/s12046-013-0119-3

2. S. Louhenkilpi, Continuous casting of steel, *Treatise on process metallurgy.* Elsevier, 2014, p 373–434

3. Y. Satoh, T. Yamamura, and T. Takimoto, Techniques for Long Life Materials Applied to Continuous Caster Roll, *Kawasaki Steel Tech. Rep.*, 2001, **45**, p 42–49

4. B.G. Thomas, Continuous casting (metallurgy), *Yearbook of science and technology.* McGraw-Hill, 2004, p 1–6

5. M. Du Toit, and J. Van Niekerk, Improving the Life of Continuous Casting Rolls Through Submerged Arc Cladding with Nitrogen-Alloyed Martensitic Stainless Steel, *Weld. World*, 2010, **54**, p R342–R349. https://doi.org/10.1007/BF03266748

6. B.G. Thomas, M.A. Wells, and J. Sengupta, The Use of Water Cooling During the Continuous Casting of Steel and Aluminum Alloys, *Metall. Mater. Trans. A*, 2005, **36A**, p 187–204

7. A. Sanz, New Coatings for Continuous Casting Rolls, *Surf. Coat. Technol.*, 2004, **177–178**, p 1–11. https://doi.org/10.1016/j.surfcoat.2003.06.024

8. G.F. Da Silva, S.S.M. Tavares, J.M. Pardal, M.R. Silva, and H.F.G. De Abreu, Influence of Heat Treatments on Toughness and Sensitization of a Ti-alloyed Supermartensitic Stainless Steel, *J. Mater. Sci.*, 2011, **46**, p 7737–7744. https://doi.org/10.1007/s10853-011-5753-8

9. K. Kishore, M. Adhikary, G. Mukhopadhyay, and S. Bhattacharyya, Development of Wear Resistant Hammer Heads for Coal Crushing Application Through Experimental Studies and Field Trials, *Int. J. Refract. Hard Met.*, 2019, **79**, p 185–196. https://doi.org/10.1016/j.ijrmhm.2018.12.009

10. L. Zhu, P. Xue, Q. Lan, G. Meng, Y. Ren, Z. Yang, P. Xu, and Z. Liu, Recent Research and Development Status of Laser Cladding: A Review, *Opt. Laser Technol.*, 2021, **138**, p 1–26. https://doi.org/10.1016/j.optlastec.2021.106915

11. W. Steen and K. Watkins, Coating by Laser Surface Treatment, *J. Phys. IV Proc. EDP Sci.*, 1993, **03**, p 581–590. https://doi.org/10.1051/jp4:1993961

12. K. Kishore, N. Jaiswal, A. Prabhakaran, and K.S. Arora, Through-Thickness Microstructure and Wear Resistance of Plasma Transferred Arc Stellite 6 Cladding: Effect of Substrate, *CIRP J. Manuf. Sci. Technol.*, 2023, **42**, p 24–35. https://doi.org/10.1016/j.cirpj.2023.01.014

13. Z. Liu, G. Lian, C. Zhao, J. Peng, and Y. Zhang, The Forming Control Method of Ni35A+ TiC Composite Coatings on Cylindrical Substrate Deposited by Laser Cladding, *J. Mater. Eng. Perform.*, 2023, **32**, p 1333–1346. https://doi.org/10.1007/s11665-022-07160-1

14. C. Navas, A. Conde, B.J. Fernández, F. Zubiri, and J. de Damborenea, Laser Coatings to Improve Wear Resistance of Mould Steel, *Surf. Coat. Technol.*, 2005, **194**(1), p 136–142. https://doi.org/10.1016/j.surfcoat.2004.05.002

15. C.T. Kwok, K.H. Lo, F.T. Cheng, and H.C. Man, Effect of Processing Conditions on the Corrosion Performance of Laser Surface-Melted AISI 440C Martensic Stainless Steel, *Surf. Coat. Technol.*, 2003, **166**(2–3), p 221–230. https://doi.org/10.1016/S0257-8972(02)00782-X

16. K. Feng, Y. Chen, P. Deng, Y. Li, H. Zhao, F. Lu, R. Li, J. Huang, and Z. Li, Improved High-Temperature Hardness and Wear Resistance of Inconel 625 Coatings Fabricated by Laser Cladding, *J. Mater. Process. Technol.*, 2017, **243**, p 82–91. https://doi.org/10.1016/j.jmatprotec.2016.12.001

17. A. Ray, K.S. Arora, S. Lester, and M. Shome, Laser Cladding of Continuous Caster Lateral Rolls: Microstructure, Wear and Corrosion Characterisation and On-Field Performance Evaluation, *J. Mater. Process. Technol.*, 2014, **214**(8), p 1566–1575. https://doi.org/10.1016/j.jmatprotec.2014.02.027

18. P. Maruschak, R. Bishchak, D. Baran, and L. Poberezhny, Failure Analysis of Continuous Casting Rolls Material and Physical Simulation of Thermal Fatigue Loading, *Mechanika*, 2013, **19**(4), p 398–402. https://doi.org/10.5755/j01.mech.19.4.5046

19. S. Lee, D.H. Kim, J.H. Ryu, and K. Shin, Correlation of Microstructure and Thermal Fatigue Property of Three Work Rolls, *Metall. Mater. Trans. A*, 1997, **28**(12), p 2595–2608. https://doi.org/10.1007/s11661-997-0017-6

20. Y. Lee, M. Nordin, S.S. Babu, and D.F. Farson, Effect of Fluid Convection on Dendrite Arm Spacing in Laser Deposition, *Metall. Mater. Trans. B*, 2014, **45**(4), p 1520–1529. https://doi.org/10.1007/s11663-014-0054-7

21. W. Chen, B. Xiao, L. Xu, Y. Han, L. Zhao, and H. Jing, Additive Manufacturing of Martensitic Stainless Steel Matrix Composites with Simultaneously Enhanced Strength-Ductility and Corrosion Resistance, *Compos. B. Eng.*, 2022, **234**, p 1–13. https://doi.org/10.1016/j.compositesb.2022.109745

22. E. Altuncu and M. Tarım, Laser Cladding of Martensitic Stainless Steels on Armor Steels, *Emerg. Mater. Res.*, 2019, **9**(1), p 55–58. https://doi.org/10.1680/jemmr.18.00120

23. P. Fasihi, O. Kendall, R. Abrahams, P. Mutton, C. Qiu, T. Schläfer, and W. Yan, Tribological Properties of Laser Cladded Alloys for Repair of Rail Components, *Materials*, 2022, **15**(21), p 1–14. https://doi.org/10.3390/ma15217466

24. Y.F. Yin and R.G. Faulkner, Physical and elastic behavior of creep-resistant steel, *Creep-resistant steels*. Woodhead Publishing in Materials, 2008, p 217–240

25. F.C. Hull, S.K. Hwang, J.M. Wells, and R.I. Jaffee, Effect of Composition on Thermal Expansion of Alloys Used in Power Generation, *J. Mater. Eng.*, 1987, **9**(1), p 81–92

26. K. Chandra and A. Kranzmann, High Temperature Oxidation of 9–12% Cr Ferritic/Martensitic Steels Under Dual-Environment Conditions, *Corros. Eng. Sci. Technol.*, 2018, **53**, p 27–33. https://doi.org/10.1080/1478422X.2017.1374049

27. V.F. De Souza, A.J. Araújo, J.L.N. Do Santos, C.A.D. Rovere, and A.M.S. De Malafaia, Kinetics Oxidation and Characterization of Cyclically Oxidized Layers at High Temperatures for FeMnSiCrNiCe and FeSiCrNi Alloys, *Mater. Res.*, 2017, **20**, p 365–373. https://doi.org/10.1590/1980-5373-mr-2017-0098

28. A.V. Makarov, A.E. Kudryashov, S.V. Nevezhin, A.S. Gerasimov, and A.A. Vladimirov, Reconditioning of Continuous Casting Machine Rollers by Laser Cladding, *J. Phys. Conf. Ser.*, 2020, **1679**, p 42–47. https://doi.org/10.1088/1742-6596/1679/4/042047

29. L.D. Conceição and A.S.C.M. D'Oliveira, The Effect of Oxidation on the Tribolayer and Sliding Wear of a Co-Based Coating, *Surf. Coat. Technol.*, 2016, **288**, p 69–78. https://doi.org/10.1016/j.surfcoat.2016.01.013

30. F. Shu, B. Wang, S. Zhang, S. Sui, X. Zhang, and J. Zhao, Microstructure, High-Temperature Wear Resistance, and Corrosion Resistance of Laser Cladded Co-Based Coating, *J. Mater. Eng. Perform.*, 2021, **30**, p 3370–3380. https://doi.org/10.1007/s11665-021-05704-5